JOURNAL OF GEOPHYSICAL RESEARCH, VOL. 88, NO. A7, PAGES 5645–5656, JULY 1, 1983

Waves Observed Upstream of Interplanetary Shocks

BRUCE T. TSURUTANI AND EDWARD J. SMITH

Jet Propulsion Laboratory, California Institute of Technology, Pasadena, California 91109

DOUGLAS E. JONES

Brigham Young University, Physics Department, Provo, Utah 84601

The properties of waves with frequencies below 3 Hz observed upstream of low Mach number (2–3) interplanetary shocks are discussed. High-frequency emissions (0.2–2 Hz in the spacecraft frame) are commonly detected immediately upstream ($<2\ R_E$) of the shocks, whereas lower frequency emissions (~ 0.05 Hz) are found to extend upstream to much greater distances (typically 10 R_E). Both emissions are right-hand circularly or elliptically polarized and generally propagate within a 15° cone angle relative to the ambient magnetic field. The lack of a significant compressional component for either of these waves is in agreement with propagation parallel to the ambient magnetic field. Upstream waves are detected principally in association with quasi-parallel shocks ($\theta_{Bn} < 65°$). Assuming the waves are propagating outward from the shock, an expression is derived for the wave frequency in the solar wind rest frame. The waves are found to have rest frame frequencies of 0.05–1 Hz and 10^{-3} to 10^{-2} Hz. Arguments are presented which exclude the possibility that the high-frequency waves are standing whistler mode waves. The most likely source of these emissions is generation at the shock by 100 eV to 1 keV electrons and propagation of the whistler mode waves into the upstream region. The lower frequency 10^{-3} to 10^{-2} Hz waves propagate at speeds near the Alfvén velocity, and hence cannot outrun the super-Alfvénic shocks. These waves must be locally generated by plasma instabilities in the upstream region. Generation by Landau electrons or ions can be ruled out due to the observation of parallel propagation of the waves. The most likely source is 1–10 keV cyclotron-resonant ions propagating away from the shock. The upstream waves bear many similarities to those observed in the earth's foreshock. The frequencies, polarization, and typical upstream extent are nearly identical. It is also deduced that the lower frequency waves of both regions are generated by keV ions streaming away from the shock. There are some differences, however. Waves upstream of interplanetary shocks are found to propagate parallel to the magnetic field ($<15°$), are noncompressive ($\Delta B/B \leq 0.25$) and are generally lower in amplitude. Additionally, there are extraordinary interplanetary events, for which the scale of the upstream wave region is greatly extended ($\sim 1300\ R_E$ or 0.04 AU) and the field takes on a more turbulent character. The latter events should be of interest in modeling Fermi acceleration of ions at collisionless shocks.

INTRODUCTION

Recent experimental observations and theoretical modeling have stressed the importance of the existence of plasma waves upstream of collisionless shocks, not only to understand the basic plasma instabilities leading to the generation of the waves, but also because there are many potential consequences of wave-particle interactions. The latter can alter the nature of the upstream region and can therefore, affect the shock structure itself. This facet of shocks is only beginning to be studied and understood (*Tsurutani and Rodriguez* [1981] and references therein). A further consequence of wave-particle interactions is that particle scattering at both upstream and downstream positions relative to the shock can effectively act as moving 'walls' of a Fermi accelerator. Significant particle energization is believed to be occurring via this process [*Jokipii*, 1966; *Teresawa*, 1979, 1981; *Fisk and Lee*, 1980; *Ellison*, 1981; *Eichler*, 1981; *Forman*, 1981; *Lee*, 1982].

It is the purpose of this paper to describe the properties of the waves that are present upstream of interplanetary, collisionless, quasi-parallel shocks. The waves are generally not detected in association with quasi-perpendicular shocks ($\theta_{Bn} > 75°$). Basic properties of the waves such as polarization, probable mode of propagation, and amplitude will be described. These emissions will be compared with the well-studied emissions upstream of the earth's bow shock.

Paper number 3A0490.
0148-0227/83/003A-0490$05.00

OBSERVATIONAL RESULTS

The ISEE 3 Jet Propulsion Laboratory (JPL) magnetometer group and the Los Alamos plasma group have attempted to identify all of the interplanetary shocks existing in the data from the time of launch (August 12, 1978) to March 1980, an interval during which solar-wind proton data are available. The normals to the shocks are calculated by the *Abraham-Schrauner* [1972] method which utilizes both plasma and field data. The upstream and downstream plasma properties, and the velocity and Mach number of the shocks, are also determined. The combined values of the shock normal angle and velocity are verified by comparing the calculated propagation times of the shocks from ISEE 3 to earth with the actual delay times obtained by using the arrival times of the shock-associated sudden commencements (SSC's) at earth. The latter measurements, taken from ground-based magnetometers, have been supplied by the World Data Center. A report of this method of study will be given in greater depth elsewhere (E. J. Smith et al., manuscript in preparation, 1983). For periods when simultaneous plasma data were not available (after March 1980), the shock normal direction was estimated using the magnetic coplanarity theorem.

High time-resolution (6 vectors per second) magnetic field data just upstream and downstream of all interplanetary shocks from launch through 1980 (over 100 events) have been examined to determined the presence (or absence) of shock-associated hydromagnetic waves. Shocks occurring in the latter half of 1980 where solar wind proton data were not available are verified by observing the occurrence of time-delayed sudden

commencements or sudden impulses. Waves were detected upstream (and also downstream) of almost all interplanetary shocks examined. The only apparent exception to this general relationship was for quasi-perpendicular shocks. Upstream waves were either significantly lower in amplitude or were not present for most of these events. Another general observation was that the upstream waves were more prominent during 1980. Because of a lack of simultaneous solar wind plasma data during the latter part of the year, it is difficult to determine the cause of this phenomenon. Possibilities are stronger shocks and/or a predominance of quasi-parallel shocks at solar maximum. A number of upstream waves from the period of study have been randomly selected and are further analyzed below.

Typical Events

Figure 1 is an example of the waves characteristic of the upstream region. The waves have the largest amplitude immediately preceding the shock, which occurs at 0925:01 UT. The waves decrease in amplitude with increasing distance from the shock. Although there are field magnitude variations associated with the waves, they are relatively small (~1.3 nT peak to peak) compared with either the amplitude of the waves (~6 nT peak to peak) or with the ambient magnetic field (~8 nT). The lack of large field compressions (<25% of wave amplitude) associated with these upstream waves is typical of the events examined in this study.

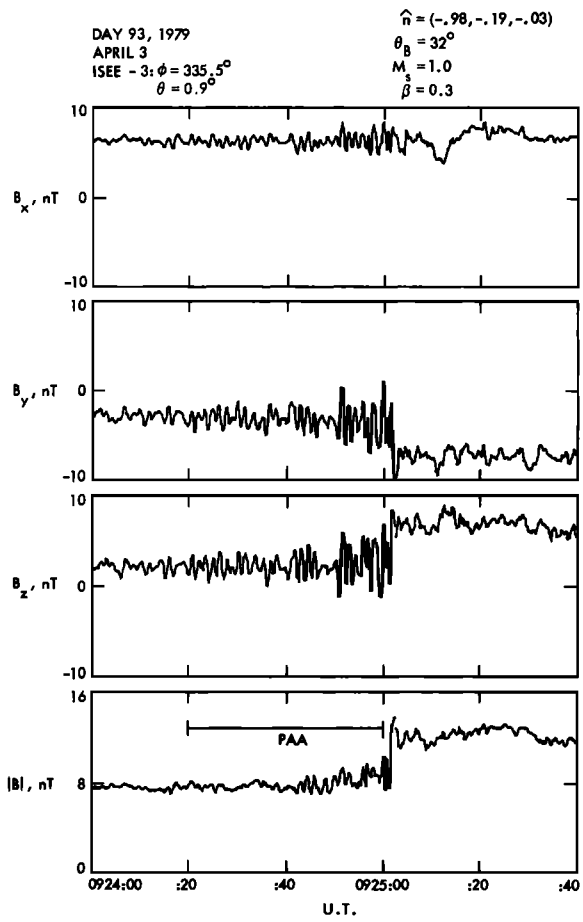

Fig. 1. Waves upstream of an interplanetary shock. The ~0.7 Hz waves have the largest amplitudes immediately preceding the shock and decrease in amplitude with increasing distance from the shock. The magnetic field magnitude variations associated with the waves are less than 25% of the wave amplitude. The interval from 0924:20 to 0925:00 UT, labeled PAA, has been subjected to a principal axis analysis. The waves are right-hand circularly polarized and propagate at an angle of 11° relative to the ambient magnetic field. Shock parameters, such as the normal direction, the normal angle relative to the upstream ambient magnetic field, the magnetosonic Mach number (V_{shock}/V_s) and upstream β ($8\pi nkT/B^2$) are given at the upper right. The ISEE 3 location is given in the upper left in terms of the azimuth and elevation angles in solar ecliptic coordinates.

These waves are propagating into a low beta plasma ($\beta \simeq 0.3$) and are associated with a low Mach number (the magnetosonic Mach number M_s is 1.0 and the Alfvén Mach number M_A is 1.1), quasi-parallel ($\theta_{Bn} = 32°$) shock. The error in the shock normal is inferred to be small, as the relative error in the calculated arrival time at earth was only 6%.

Another striking example of large amplitude, coherent waves, is shown in Figure 2. The emissions have the largest amplitude close to the shock, at 0156:35 UT. However, the waves do not simply monotonically decrease in amplitude with greater distance from the shock, as was the case in Figure 1. There are other large amplitude wave packets further upstream, as indicated by the event at 0155:00–0155:20 UT. The magnetic field magnitude variations are small for both wave packets.

The wave k vector and polarization were determined from a variance analysis of the magnetic field variations. The analysis used is equivalent to that first employed by *Sonnerup and Cahill* [1967] to determine the normal to the terrestrial magnetopause. This method has been previously used to analyze extremely low frequency (ELF) electromagnetic waves in and near the magnetosphere: plasmaspheric hiss [*Thorne et al.*, 1973], chorus [*Burton and Holzer*, 1974], and lion roars [*Smith and Tsurutani*, 1976]. *Hoppe et al.* [1981] have applied the analysis method to MHD waves in the earth's foreshock. The interval used in the analysis is indicated in Figure 2 as the third principal axis analysis (PAA) interval, from 0156:15–0156:33 UT. The waves within the interval are found to be right-hand circularly polarized, planar, and are basically propagating along the magnetic field direction ($\theta_{kB} = 11°$). The characteristic properties of these waves are given in Table 1. The properties of the waves in the other two PAA intervals are similar to the above event. These are also given in Table 1.

In Figure 3, the magnetic field for this event is displayed in the principal axis coordinate system. Axes 1, 2, and 3 correspond to the maximum, intermediate, and minimum variance directions. The field component in the minimum variance direction, B_3, is large and nearly constant, indicating a well-determined minimum variance direction. The wave field variations along the B_1 and B_2 axes have magnitudes that are approximately equal, indicating the waves are circularly polarized.

The nature of the waves is more clearly revealed by plotting the principal axes field components as functions of each other, as in Figure 4. The hodogram in the left-hand panel, in which B_2 is plotted against B_1, represents the rotation of the tip of the perturbation field in the plane of the wave. The ambient magnetic field is directed out of the paper. The interval which starts at 0156:15 UT, is indicated by B (for beginning) and E (for end). This interval corresponds to the third PAA interval of Figure 2. From the left-hand panel of Figure 4, it is quite apparent that the waves are right-hand circularly polarized. From the right-hand panel, it is observed that the wave perturbation vector remains essentially within a plane.

Analyses of the other two PAA intervals studied on this day led to similar results. The waves were right-hand circularly polarized and were propagating in a direction nearly parallel to the ambient magnetic field.

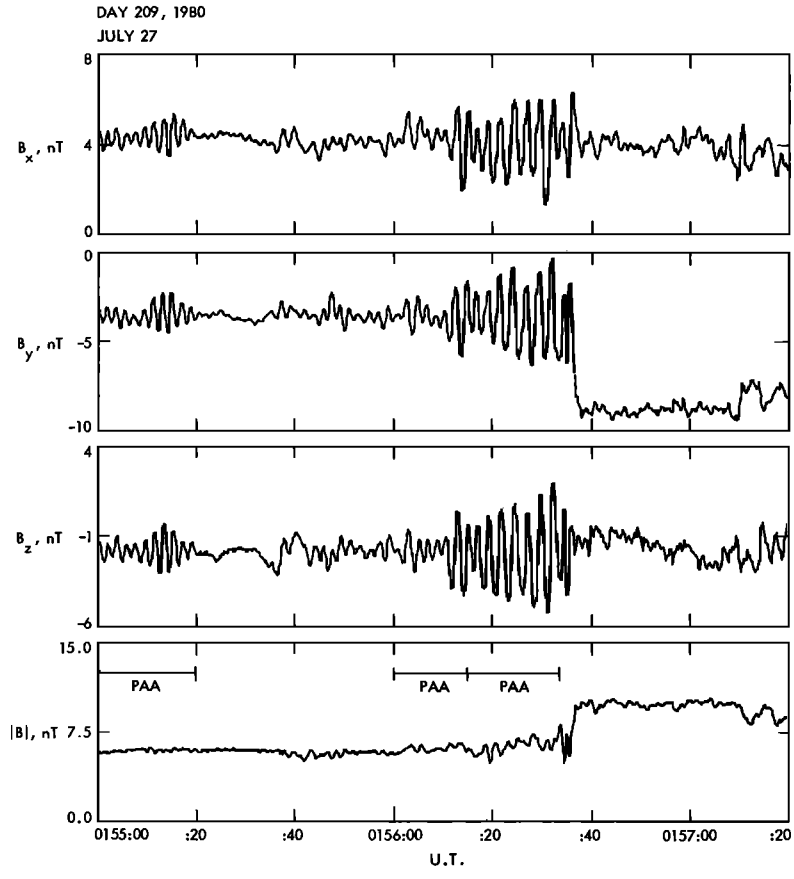

Fig. 2. Same format as in Figure 1. The wave frequencies of the three PAA intervals vary from 0.42 to 0.53 Hz, are right-hand circularly polarized and propagate in a direction nearly parallel to the magnetic field (within 3° to 11°).

Another upstream wave feature which was fairly common for many events was the presence of high-frequency waves just adjacent to, but upstream of, the shock. An example is presented in Figure 5. Large amplitude ~1 Hz waves are present from 1039:48 to 1039:55 UT. These emissions are significantly different from the 5- to 10-s waves detected further upstream of the shock. They have higher frequencies and have a significantly greater compressional component. These large-amplitude (2.7 nT peak to peak) emissions are propagating at a substantial angle to the magnetic field ($\theta_{kB} = 41°$) in accord

TABLE 1. Upstream Wave Properties

Date	Time, UT	Θ_{kB}	Peak to Peak Amplitude, nT	Polarization	λ_1/λ_2	f_{sc}	f_{sw}	θ_{kn}	θ_{Bn}	M_s	β
D239, 1978	0203:00–0206:00	5°	3.7	?	1.4	0.027 Hz	0.0031	38°	39°	3.2	3.0
	0209:00–0210:00	1°	2.8	?	1.7	0.022	0.0029	44°			
D282, 1978	0236:00–0236:17	10°	1.0	r.h.	1.15	1.4	0.542	64°	67°	1.7	0.95
D312, 1978	0108:06–0110:00	8°	5.0	r.h.	1.6	0.133	0.047	44°	49°	2.2	0.5
D316, 1978	0015:00–0018:00	4°	6.5	r.h.	1.6	0.089	0.022	24°	22°	4.7	0.5
	0022:00–0025:00	8°	8.0	r.h.	1.95	0.056	0.013	29°	21°		
	0029:00–0031:00	4°	15.5	?	2.0	0.067	0.031	46°	50°		
D068, 1979	0721:24–0721:36	20°	1.7	?	2.1	2.6	1.162	57°	53°	1.7	1.5
D093, 1979	0924:20–0925:00	11°	1.7	r.h.	1.06	0.7	0.196	34°	32°	1.02	0.29
D193, 1979	1129:50–1130:02	14°	4.0	r.h.	1.32	0.9	0.208	89°	78°		
D072, 1980	1550:20–1551:05	4°	2.0	r.h.	1.05	0.15	0.022	11°	13°		
D209, 1980	0156:05–0156:15	7°	4.0	r.h.	1.02	0.47	0.102	63°	60°		
	0156:15–0156:33	11°	6.0	r.h.	1.12	0.42	0.095	52°	63°		
	0155:00–0155:20	3°	2.5	r.h.	1.06	0.53	0.113	57°	59°		
D314, 1980	1038:00–1039:40	2°	1.5	r.h.	1.24	0.16	0.031	77°	79°		
	1039:40–1039:54	41°	2.7	r.h.	1.15	1.70	0.506	37°	77°		

The wave characteristics are given in the third through the ninth columns: the angle between the wave propagation direction and the ambient magnetic field, the peak-to-peak amplitude, the sense of polarization relative to **B**, the ratio of the maximum to intermediate eigenvalues obtained from a principal axis analysis, the wave frequency in the spacecraft reference frame, the wave frequency in the solar wind rest frame, and the wave propagation direction relative to the shock normal direction. The last three columns in the table are shock parameters, where available: the shock normal angle relative to the upstream magnetic field, the magnetosonic Mach number, and the upstream plasma beta.

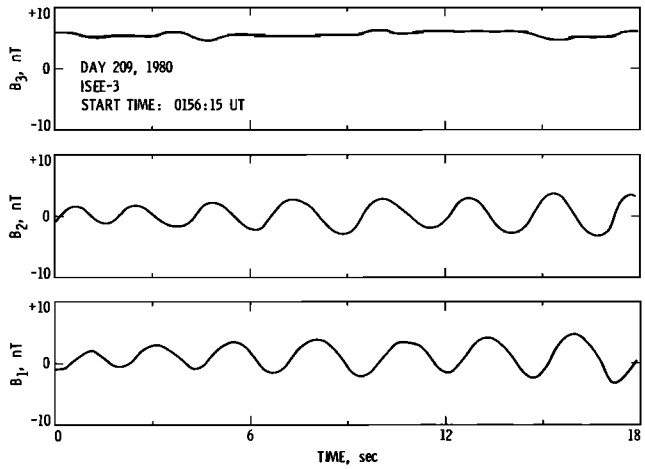

Fig. 3. The magnetic field variations during the third interval of Figure 2 (0156:15–0156:33 UT) in principal axis coordinates. Axes 1, 2, and 3 correspond to the maximum, intermediate, and minimum variance directions. The nearly constant B_3 value indicates a well-determined minimum variance direction. The approximately equal magnitude of the oscillations in B_1 and B_2 and their phase difference of 90° indicate that the waves are circularly polarized. The absence of a significant variation in field magnitude implies propagation along the ambient field direction.

with the observation of relatively large fluctuations in field magnitude.

The lower frequency waves which extend to larger distances from the shock are similar to those illustrated in Figures 1–4. They are right-hand polarized and propagate at an angle of 2° relative to the magnetic field. The ratio of the maximum to the intermediate eigenvalue is $\lambda_1/\lambda_2 = 1.24$, indicating slightly elliptical polarization.

Another example of high-frequency waves immediately upstream of interplanetary shocks is shown in Figure 6. The wave amplitudes are largest just adjacent to the shock and decrease with increasing distance from the shock. At a distance ~12,000 km in front of the shock (assuming a solar wind speed of 400 km/s), the wave amplitudes are no longer measurable. The wave frequency in the spacecraft frame is $\simeq$ 2.6 Hz. The minimum variance direction is 20° from the magnetic field orientation. Because the wave frequency is greater than the Nyquist frequency of the data (3.0 Hz), the sense of rotation of the waves cannot be determined.

In the above figure, waves are also present in the region downstream of the shock. The largest amplitudes are detected just adjacent to the shock and decrease with increasing distance. Within 20 s after the passage of the shock (a distance equivalent of ~12,000 km), the wave amplitudes have decreased to background solar wind fluctuation levels and can no longer be identified. The downstream wave frequencies are again greater than 3.0 Hz preventing polarization determinations.

Extraordinary Events

The previous examples (Figures 1–6) have been shown to illustrate typical upstream wave features associated with interplanetary shocks. Both the high-frequency waves detected just adjacent to the shock and the lower frequency waves which extent to greater distances from the shock are coherent, generally propagate along the magnetic field (however, Figure 5 is an exception), and are right-hand polarized in the spacecraft frame. The high-frequency emissions typically extend only a few tens of seconds ($< 10^4$ km) upstream of the shock, whereas the lower frequency waves are found several minutes (5–7 × 10^4 km or 8–12 R_E) into the upstream region.

There are, however, cases where the associated wave properties are considerably different from the 'typical' picture that is presented above. These events are beginning to attract a great amount of attention because of the anomalously large energetic proton events associated with the waves and/or the shocks. Three such wave events occurred on November 11–12, 1978, February 11, 1979, and March 1, 1979. One event will be discussed briefly to illustrate the wave features, and to contrast them to the 'typical' case. Because they are relatively rare events, we will not dwell on their features at this time, but will postpone detailed discussions to future wave-particle interaction papers.

Figures 7 and 8 illustrate examples of the waves associated with the event on November 11–12, 1978. Figure 7 illustrates the upstream and downstream waves associated with this quasi-parallel shock event ($\theta_{Bn} = 22°$). The details of the shock parameters (and the associated higher frequency (ELF-VLF) plasma waves not shown) have been discussed previously by *Kennel et al.* [1982]. The error in the estimated arrival time of the shock at the earth is only 5%. *Russell et al.* [1983] have analyzed this event using three spacecraft and have determined an average shock normal angle of 40° and a lower Mach number of 2.2.

Large amplitude (6 nT peak to peak), slightly compressional ($\Delta|B|/|B| \sim 0.1$–0.2) waves of ~7-s period are present upstream of the shock. The fluctuations in the interval from 0026:20 to 0027:00 UT have been analyzed to determine the characteristics of the waves. The emissions are found to be elliptically polarized, with $\lambda_1/\lambda_2 \simeq 1.9$, and propagating along the magnetic field with $\theta_{kB} = 7°$. The ratio of the intermediate to minimum eigenvalue, λ_2/λ_3, is 13.0, indicating a well-determined event. The sense of polarization of these upstream waves is not clear from the analysis of this interval.

Even larger amplitude quasi-periodic waves are present downstream from the shock. Just adjacent to the shock (0028:19–0028:30 UT), ~20 nT peak to peak, ~3-s waves are detected. These emissions are elliptically polarized ($\lambda_1/\lambda_2 = 2.4$) in a right-hand sense and are propagating nearly parallel to the ambient field, $\theta_{kB} = 12°$. For this event, λ_2/λ_3 is equal to 4.4.

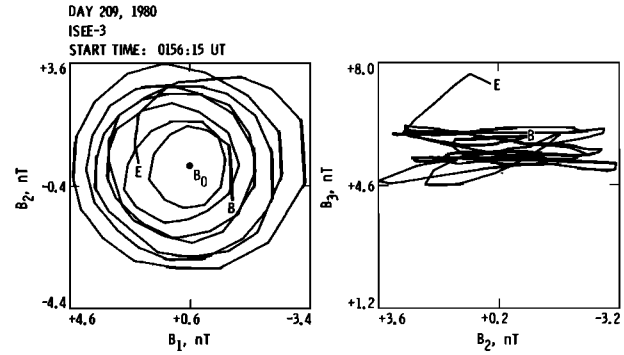

Fig. 4. Polarization plots for the event in Figure 3. The left-hand panel represents the rotation of the tip of the perturbation vector in the plane of the wave. The ambient magnetic field, $\mathbf{B}_0$, is directed out of the paper. The beginning of the event is indicated by B and ends at E. The waves are right-hand circularly polarized. The right panel, a plot of B_3 versus B_2, shows that the perturbation field lies principally in the B_1–B_2 plane.

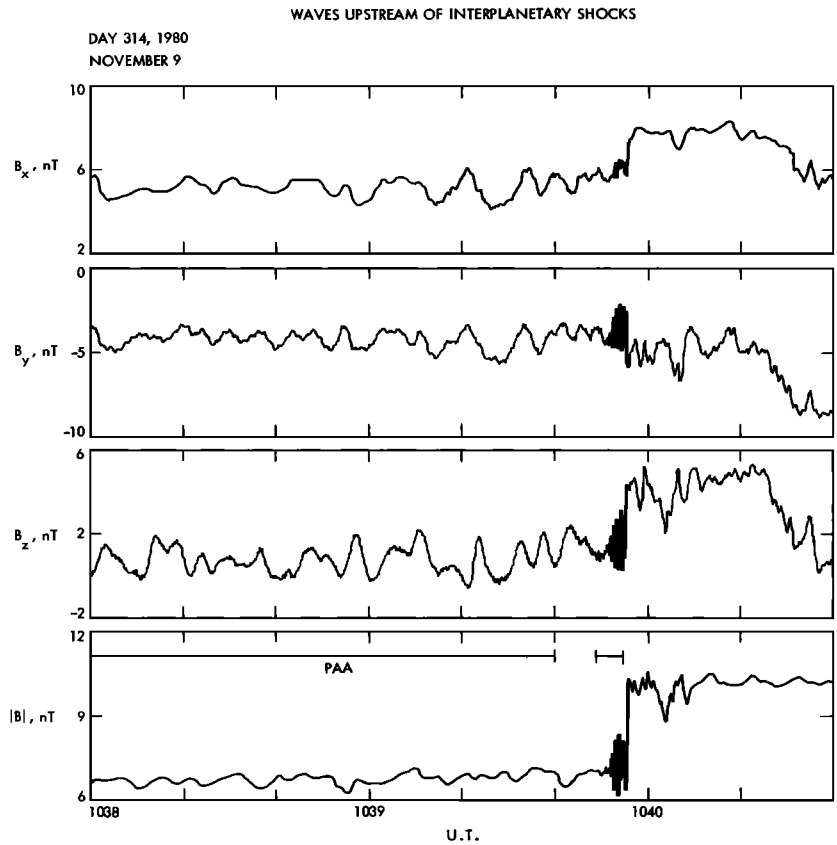

Fig. 5. An example of high-frequency waves ($f \simeq 1.7$ Hz) just adjacent to, but upstream of, an interplanetary shock. These emissions are detected from 1039:48 to 1039:55 UT. The emissions are right-hand circularly polarized and are propagating at an angle of 41° relative to the magnetic field. The significant compressional variations associated with these waves is due to the large angle of propagation. Lower frequency emissions ($f \simeq 0.16$ Hz) are detected further upstream of the shock. As in previous figures, these emissions are right-hand circularly polarized and are propagating along the magnetic field ($\theta_{kB} = 2°$).

Further from the shock in the downstream region, in the third interval labeled PAA (0029:20–0031:00 UT), ~20-s quasi-periodic waves are detected. These waves are elliptically polarized ($\lambda_1/\lambda_2 = 1.9$) and are again found to be propagating parallel to the ambient field, $\theta_{kB} = 5°$. The ratio λ_2/λ_3 is 5.4. The sense of polarization is difficult to ascertain but is primarily right-handed. These large amplitude (> 10 nT) waves are essentially noncompressive.

Upstream waves are detected continuously to much greater distances in front of the shock than shown in Figure 7. Emissions at 1900 UT of the previous day (November 11, 1978) imply that the scale of the upstream wave region corresponds to ~1300 R_E or 0.04 AU. The region of enhanced wave activity is approximately coincident with an energetic particle event (K. A. Anderson and R. P. Lin, personal communication, 1982). An example of the emissions detected 350 R_E upstream of the shock are shown in Figure 8. Although it is clear that large-amplitude turbulence is present, clear quasi-periodic structure, such as shown in previous figures, is, in general, absent. There is a possibility that this entire region is composed of many superposed wave packets, causing the field to have a disordered appearance.

The entire interval in addition to two short intervals within Figure 8 have been analyzed separately to determine the properties of the magnetic fluctuations. A principal axis analysis of the entire interval indicated that the minimum variance direction is along the average field direction, but no clear sense of rotation was found. Thus two shorter intervals, 2300:20–2301:00 UT and 2303:00–2304:00 UT, were additionally examined. These two intervals had oscillations within the interval, leading the authors to the hope that a clear polarization would be found.

The ratio of the eigenvalues, λ_1/λ_2, are found to be large in each case, 2.6 and 1.7, respectively, indicating elliptical polarization. The waves are highly planar, as indicated by large ratios for λ_2/λ_3 (29 and 7.7, respectively). In neither case could a clear sense of rotation be found. Evidence for both linear and right-hand rotation were present in each data interval. Although the field is highly turbulent, the direction of minimum variation was surprisingly close to the average field direction. The values for θ_{kB} are 2.5° and 3.0°, respectively.

Several other periods of the event of day 315–316, 1978, which were observed upstream within 15 min of the shock, were studied. Although the sense of polarization was not always clear, there were periods where right-hand polarization waves were obviously present. Three of these periods are indicated in Table 1.

The power spectral density of the waves for the November 11–12, 1978, event has been determined by applying a fast Fourier transform to 1024 values of the high-resolution data (6 per second) at a time. The composition spectra shown in Figure 9 are formed by adding spectra for consecutive intervals to give ~30-min values. The power spectra for the x, y, z components and field magnitude are illustrated in the figure. Figures 9*a*

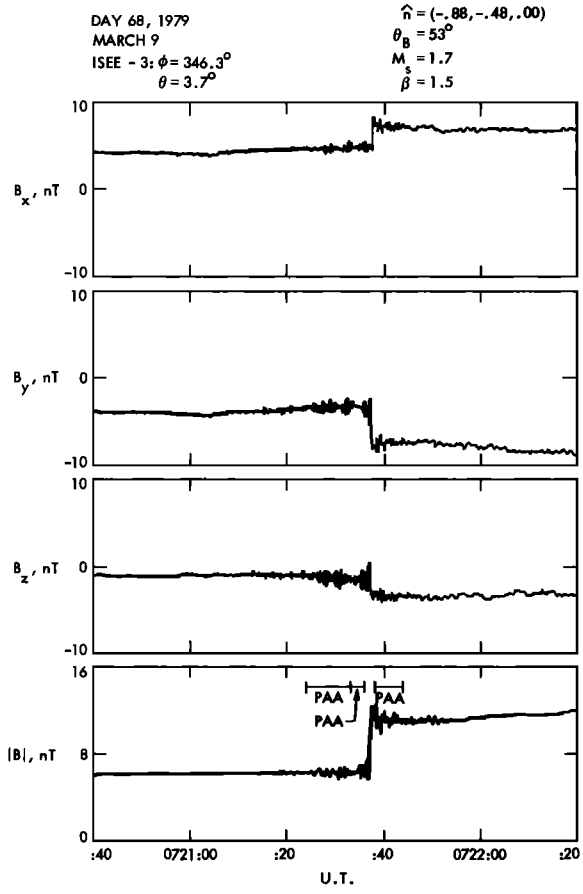

Fig. 6. Another example of high-frequency (2.6 Hz) waves immediately upstream of an interplanetary shock. High-frequency waves are also detected immediately downstream of the shock.

through 9*d* represented a time sequence of the wave power from 61 to 88 min upstream of the shock (Figure 9*a*) to 2–30 min downstream of the shock (Figure 9*d*). The fluctuation power associated with the shock itself is not included in any of the panels in Figure 9. Each spectrum has a bandwidth of 5.9×10^{-3} Hz. The number of degrees of freedom is 38, 40, 36, and 34 for Figures 9*a* through 9*d*, respectively.

In the top panel, the wave power was averaged over the period 2300–2327 UT, day 315. It is noted that the B_y and B_z spectra are approximately equal in magnitude and are distinctly greater than the B_x spectrum, which in turn is greater than the $|B|$ spectrum. The above differences are approximately one half order of magnitude (in power) at the highest frequency displayed ($\sim 5 \times 10^{-1}$ Hz) and slightly greater at the low frequency end. The large and significant difference between the B_y and B_z spectra and the B_x spectrum can be explained by the unusual field orientation for this period. The average ambient magnetic field is almost completely in the x direction for the entire event (see *Tsurutani et al.* [1983] for a more detailed discussion), thus indicating that there is considerably more power associated with the transverse oscillations than with fluctuations along the magnetic field direction. The same explanation holds for the observation of greater power associated with the B_x component relative to the $|B|$ fluctuations.

The general shapes of the four spectra are very similar. Each is broad and shows no sharp peaks throughout the range illustrated. The spectral intensities slowly decrease with increasing frequencies. The spectra have an apparent slope change near 5×10^{-2} Hz, a characteristic frequency for the 'typical' upstream long-period waves illustrated previously. There appears to be no simple mathematical relationship which can describe the above spectral shapes.

As the spacecraft gets closer to the shock (Figures 9*b* and 9*c*) the intensity of the waves increases significantly. By 0000–0025 UT (Figure 9*c*), the region immediately upstream of the shock, the wave intensity has grown by approximately a factor of 3. The increase is greatest at high frequencies and least at the lower end of the spectra, thus causing the spectra to flatten as the spacecraft nears the shock. The relative differences between the B_y or B_z and the B_x spectra, and also between the B_x and the $|B|$ spectra, as discussed with Figure 9*a*, are still present.

The most dramatic change in the wave spectra occurs as the shock is crossed. The bottom panel, Figure 9*d*, contains the average wave spectra for a time interval which begins several minutes after shock passage. The spectra are almost straight lines, indicating power law fits. It is found that the B_x, B_y, B_z, and $|B|$ spectra can be represented by $I_x = 0.112 f^{-1.71}$, $I_y = 0.148 f^{-1.72}$, $I_z = 0.176 f^{-1.84}$, and $I_{|B|} = 0.036 f^{-1.81}$ nT^2/Hz. There is only a factor of about 4 between the B_y and B_z spectra and the $|B|$ spectra, implying a significant increase in the compressional component of the waves for this period.

Summary of Wave Observations

A summary of the results of the waves studied in detail is given in Table 1. The values of θ_{kB} indicate that these emissions are propagating essentially parallel to the ambient magnetic field. This is consistent with the finding that there is little or no variation in magnetic field magnitude associated with the emissions. With only a few exceptions (primarily the high-frequency waves adjacent to the shock), the waves appear to be propagating within a cone angle of $\sim 15°$ to the ambient field. Because the solid angle subtended by this cone is less than 4% of the hemisphere, the waves are essentially propagating along **B** (see arguments in *Smith and Tsurutani* [1976]). In comparison, the wave direction of propagation relative to the shock normal angle θ_{kn} is also tabulated. The waves are not propagating in a direction orthogonal to the shock plane or at any ordered direction relative to the shock surface. The wave propagation direction seems to be best ordered when compared to the upstream magnetic field direction.

For all cases where the polarization could be determined, the waves were found to be right-hand polarized in the spacecraft frame (except for the extraordinary events discussed). The only exceptions to the above occurred when the wave frequency was approaching the Nyquist frequency (3.0 Hz), and the polarization could not be determined. The ratio of the maximum to intermediate eigenvalues, λ_1/λ_2, indicates that the waves are, in general, circularly or elliptically polarized.

Upstream waves are almost always associated with shocks that are quasiparallel or oblique in nature ($\theta_{kn} < 65°$). Waves are generally not detected in association with quasiperpendicular shocks, although exceptions have been found. For the latter events, the wave amplitudes are generally lower. There are several possible reasons for this observation. For large shock-normal angles, the waves or the particles responsible for generating the waves must travel large distances along the magnetic field to get substantially upstream of the shock. Thus if such waves are present, they perhaps should be detected only very close to the shock itself. Wave events such as illustrated in Figure 5, where a high-frequency component was detected just adjacent to the shock, support this hypothesis.

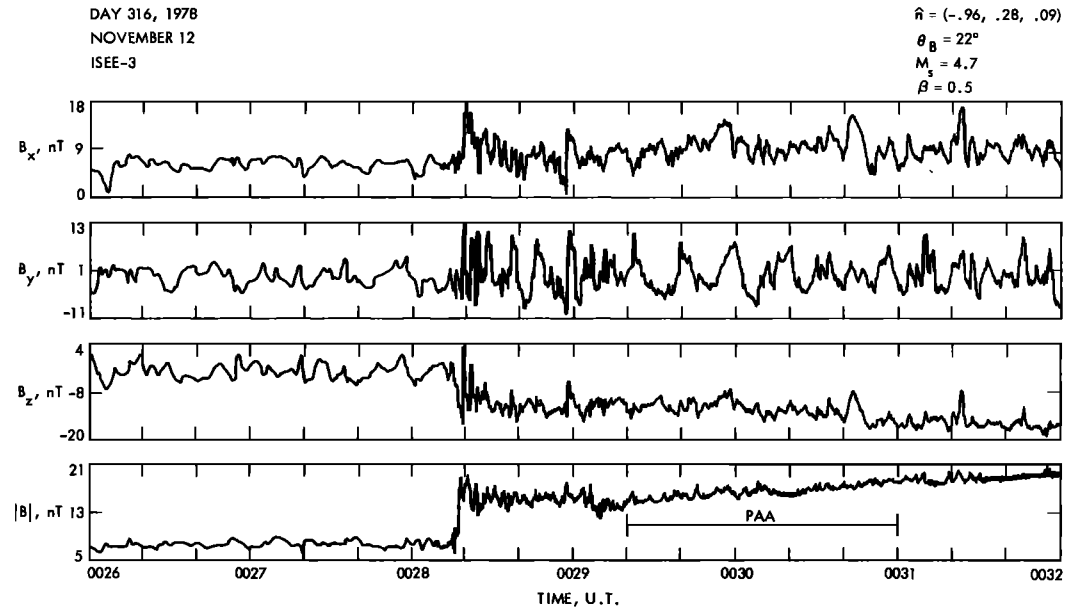

Fig. 7. Large amplitude upstream and downstream waves associated with a quasi-parallel shock on November 12, 1978. The upstream waves have a ~7-s period, are elliptically polarized ($\lambda_1/\lambda_2 = 1.9$), and are propagating nearly parallel to the magnetic field. The sense of polarization of these waves is uncertain. The downstream waves have periods of ~3 s, are right-hand elliptically polarized and are propagating nearly parallel to the magnetic field ($\theta_{kB} = 12°$). Waves are present to unusually large distances upstream of the shock, $\simeq 1300\ R_E$ or 0.04 AU. A large proton event with energies extending from 60 keV to 5 MeV is coincident with the upstream waves (R. P. Lin, personal communication, 1982).

Another obvious possibility is that quasi-perpendicular shocks do not directly or indirectly generate upstream waves.

Wave Properties in the Solar Wind Frame

The frequencies of the waves given in Table 1 are measured relative to the spacecraft frame. To identify the instability generating the waves and any potential wave-particle interactions, knowledge of the frequency in the 'solar wind frame' is required. Without the aid of a two-spacecraft technique [*Hoppe et al.*, 1981], simultaneous wave electric field or high time resolution plasma measurements (most of these wave frequencies are too high for current plasma instrumentation), the absolute direc-

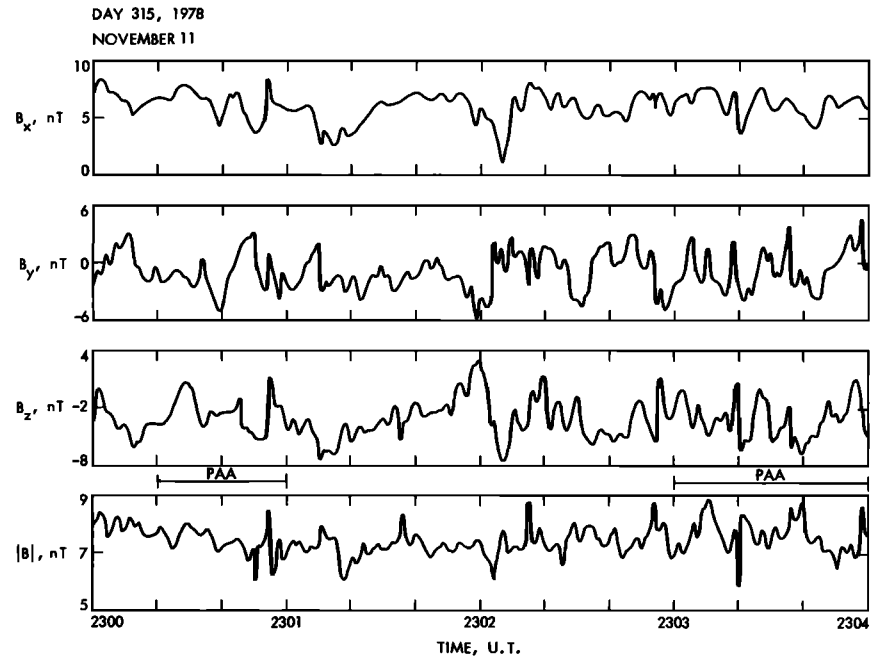

Fig. 8. An example of waves ~350 R_E upstream of the shock which was shown in the previous figure. The fields are very turbulent and give no clear indication of a preferred sense of rotation. Principal axis analyses of several intervals indicate the wave perturbations have principal eigenvalue ratios of $\lambda_1/\lambda_2 = 1.7$–2.6 with the minimum variance direction along the average ambient magnetic field direction ($\theta_{kB} < 3°$).

tion of wave propagation (away from the shock or toward the shock) and hence the intrinsic wave polarization, cannot be ascertained. However, if one uses the knowledge gained from the ISEE 1 and 2 bow shock studies, i.e., assumes that the waves

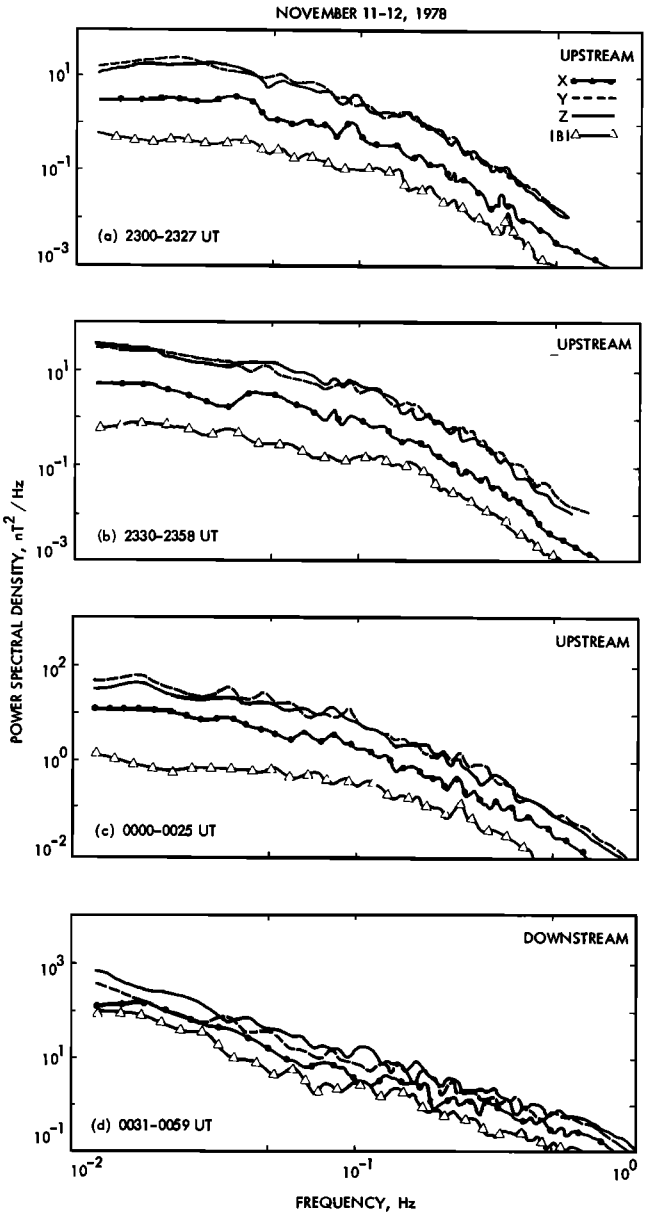

Fig. 9. Power spectra for the November 11–12, 1978, event. The PSD for frequencies from 10^{-2} to 10^{0} Hz were derived by using a standard FFT technique. Each spectrum was obtained is over a ~ 30-min interval. Time increases from the top (Figure 9*a*) to the bottom (Figure 9*d*). The top panel illustrates the broad wave spectrum centered at about 5×10^{-2} Hz which is present from 2300 to 2327 UT. The B_y and B_z spectra have higher intensities (by ~3 times) than the B_x spectrum. This feature can be explained by noting that the field lies principally in the x direction. If the waves are propagating along B and are predominantly transverse (as has been shown in previous examples), the wave fluctuations will be primarily in the y or z direction. The wave intensity increases as the shock approaches the spacecraft. In Figure 9*c* just upstream of the shock, the wave intensity is ~3 times greater than in Figure 9*a*. The increase is greater at the highest frequencies, which causes the spectra to flatten. After shock passage (Figure 9*d*), the waves become more intense and the spectra takes a power law shape, with $I \propto f^{-1.7}$ to $f^{-1.8}$. There is significantly more wave compressional power in the postshock region than in the upstream region.

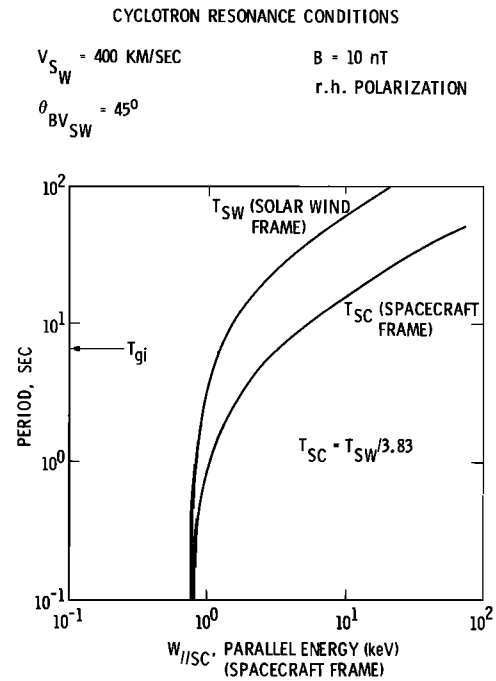

Fig. 10. Cyclotron resonance conditions between energetic protons and right-hand circularly polarized waves. A cutoff occurs when f_{gi}/f approaches zero. This arises when the particle velocity equals the wave velocity and anomalous Doppler-shifted cyclotron resonance can no longer occur. Assuming a 45° magnetic field angle relative to the solar wind velocity, the cutoff occurs at ~1 Hz, below which protons do not resonantly interact with the waves. 1–10 keV protons are resonant with the waves discussed in this paper.

are propagating away from the shock (M. M. Mellott, private communication, 1982), the rest frame frequency (and wave phase velocity, etc.) can be calculated.

If the waves are propagating away from the shock in the same direction as the solar wind flow (but along **B**), the waves should always be detected in their true sense of polarization. Because the two velocities, V_{ph} and V_{sw}, are in the same general direction, the detected wave polarization should never be reversed. This is entirely consistent with the results presented in this paper. Only one sense of polarization has been detected (right-hand).

For the case of the earth's foreshock, the waves are propagating upstream of a reverse shock, against the flow of the solar wind. If the upstream component of the wave phase speed is greater than the solar wind speed, the waves will be detected with their true sense of rotation. However, if the solar wind speed is the larger, there will be an anomalous Doppler shift and the waves will be detected with the opposite polarity. This feature has led to great difficulty in analyzing the waves of the foreshock region.

Thus, making only the simple assumption that the waves are propagating away from the shock (which is consistent with observations), all the other properties of the waves can be determined. The cold plasma dispersion relation for parallel propagating right-hand waves is given by *Stix* [1962]:

$$k^2c^2/(2\pi)^2f^2 = (f^2 - ff_{ge} - f_{ge}f_{gi} - f_{pe}^2)/(f + f_{gi})(f - f_{ge}) \quad (1)$$

where f, f_{ge}, f_{gi}, and f_{pe} are the wave, electron gyro, ion gyro, and electron plasma frequencies (in units of hertz), respectively, and c is the velocity of light. Since the index of refraction,

$n = kc/2\pi f$, is much greater than unity in the solar wind and $f \simeq f_{gi} \ll f_{ge} \ll f_{pe}$, the above expression can be simplified to

$$V_{ph}^2 \simeq V_A^2(1 + f/f_{gi}) \quad (2)$$

where V_{ph} and V_A are the wave phase velocity ($2\pi f/k$) and the Alfvén velocity, respectively. Assuming an outward propagating wave, the Doppler shift relationship is

$$f_{sc} = f_{sw}(V_{ph} + V_{sw} \cos \theta_{kV})/V_{ph} \quad (3)$$

where f_{sc}, f_{sw} are the wave frequencies in the spacecraft and the solar wind reference frames, V_{sw} is the solar wind velocity, and θ_{kV} is the angle between the wave direction of propagation and the solar wind velocity vector. Combining equations (2) and (3), we get an expression for the wave frequency in the solar wind (rest) frame.

$$f_{sc} \simeq f_{sw}[V_A(1 + f_{sw}/f_{gi})^{1/2} + V_{sw} \cos \theta_{kV}]/V_A(1 + f_{sw}/f_{gi})^{1/2} \quad (4)$$

The above equation has been solved exactly by computer for each individual case. By using the measured solar wind velocity, plasma density, and magnetic field strength, the wave frequency in the solar wind frame, f_{sw}, has been computed and is listed in Table 1. For typical wave frequencies of 0.05 Hz and 0.2–2 Hz measured in the spacecraft frame, the waves have frequencies of 10^{-2} Hz and 0.05–1 Hz in the solar wind frame.

Comparison to Waves in the Earth's Foreshock

The waves detected upstream of interplanetary shocks have a great many similarities to those detected in the upstream region of the earth's bow shock, even though the bow shock occupies a different portion of parameter space. The bow shock is almost always supercritical with a Mach number of 8–12, whereas interplanetary shocks are subcritical (Mach numbers $\leq$ 3). In spite of this major difference, the similarity between the waves is striking. The wave rest-frame frequencies of 0.5–10 f_{gi} and 10^{-1} f_{gi} are similar to those detected upstream of the bow shock. Both higher frequency, f = 0.5–4 Hz [*Heppner et al.*, 1967; *Olsen et al.*, 1969; *Russell et al.*, 1971; *Fairfield*, 1974; *Hoppe et al.*, 1982], and lower frequency, ~20 to 60-s [*Fairfield*, 1969; *Hoppe et al.*, 1981; *Hoppe and Russell*, 1982] emissions are prominent features of the earth's foreshock. In the solar wind frame, these emissions have frequencies 0.1–40 f_{gi} and ~7 $\times 10^{-2}$ f_{gi}, respectively, in close correspondence with the values reported here. The assumption of wave propagation away from the shock is consistent with the detection of only right-hand polarized waves, again analogous to the foreshock waves. The typical scale of the upstream region is also similar. The interplanetary waves are typically detected several minutes ahead of the shock. Assuming an average solar wind speed of 400 km/s, the waves are present ~8 R_E upstream of the shock, a distance comparable to the foreshock scale.

Even the scale of the extraordinary event presented in this paper has similarities with the earth's foreshock region. It has demonstrated that waves are present throughout a 0.04 AU distance upstream of an interplanetary shock. *Sanderson et al.* [1982] have reported locally generated waves associated with sunward streaming ions at ISEE 3, a distance of 0.01 AU upstream of the bow shock. It remains to be determined if turbulent fields can be detected closer to the bow shock by ISEE 1 and 2 similar to those displayed in this paper for an interplanetary shock.

There are a few differences between the waves addressed in this study and those upstream of the bow shock. There is a lack of a significant compressional component in the waves upstream of interplanetary shocks. This difference is explained as simply being due to a difference in the wave direction of propagation relative to the ambient magnetic field. The waves discussed in this paper are propagating parallel to the magnetic field, whereas cross-field propagation (θ_{kB} = 20°–45°) is more typical for the lower frequency foreshock waves [*Hoppe et al.*, 1981].

Another slight difference, important for wave-particle interaction calculations, is that the interplanetary shock-associated upstream waves are lower in amplitude than the foreshock waves. Interplanetary shock-associated waves can sometimes be as large as $\Delta B/B_0 \simeq 0.5$, but they are typically considerably less, as indicated in Table 1. Values of $\Delta B/B_0 \sim 1$ have been cited as typical for the foreshocks by *Hoppe et al.* [1981]. Large amplitude (compressional) waves have been detected in interplanetary events (*Tsurutani et al.* [1982]) at 5 AU, but they are the exception rather than the rule.

WAVE GENERATION REGIONS AND MECHANISMS

There are several potential sources of either of the waves: generation at the shock, generation near the shock plus upstream propagation, and local upstream generation. Of these three, it can be demonstrated that for waves detected just adjacent to the shock, standing whistler mode waves can be ruled out. Generation at the shock plus upstream propagation is the most likely explanation. For the longer period waves detected well away from the shock, local upstream generation is the only possible explanation.

Theoretical studies [*Biskamp*, 1973; *Karpman*, 1964] have postulated that circularly polarized whistler mode (right-hand) waves, which are stationary relative to the shock frame, may be present in the region upstream of shocks. *Perez and Northrop* [1970] and *Tidman and Krall* [1971] have predicted the amplitude and polarization of the upstream and downstream waves by assuming a steady thin current sheet associated with a low Mach number, low β, laminar shock. The experimental results of *Fairfield and Feldman* [1975], who studied the regions upstream of low Mach number (1.2–2.0) bow shocks (which occurred when either the solar wind density was low or the magnetic field strength was high), established the existence of such waves with 6- to 130-s periods. *Fairfield and Feldman* [1975] demonstrated that the wave normal and shock normal were parallel and the waves were right-hand circularly polarized when approaching the shock from the upstream side and left-hand circularly polarized when moving in the opposite sense. The wave amplitudes were found to be consistent with theory.

Similar comparisons demonstrate that the waves studied in this paper are not standing waves. The results, given in Table 1, show that wave propagation is not in a direction orthogonal to the shock plane (current sheet), but along **B** (at ~45° relative to the shock normal). The wave amplitudes were also compared with the theoretical predictions for standing waves given by the relationship: $B_w/B_0 \approx \simeq A \cos \theta_{Bn}[\beta/(M_A^2 - 1)]^{1/2}$ [*Tidman and Krall*, 1971]. In the above expression, the constant A is equal to 21.4 if $T_e = T_i$ and is 0.7 if $T_e \gg T_i$. The value for A that corresponds to the wave events of this paper is $A \simeq 0.18$, well outside the range of reasonable ion temperature to electron temperature ratios. In comparison, *Fairfield and Feldman* [1975] obtained a value of A = 3.7, which is in reasonable accord with solar wind observations.

Some of the upstream waves, particularly those with the highest frequencies, could be generated near the shock and could propagate into the upstream region without being overtaken by the shock. The short period (1–20 s) emissions, typically detected only in the region immediately adjacent to the shock, are consistent with this picture (assuming rapid wave damping). Similar high-frequency waves (1–5 Hz) have been detected just upstream of the earth's bow shock [*Holzer et al.*, 1972; *Fairfield*, 1974].

For the longer period waves ($\sim 10^{-3}$ to 10^{-2} Hz), it is easily demonstrated that propagation into the upstream region is impossible. From equation (2), assuming a typical interplanetary field strength of 10 nT (and an ion gyrofrequency of 1.6×10^{-1} Hz), it can be shown that the wave phase velocity is essentially the Alfvén speed. Because the waves are propagating at large angles relative to the shock normal direction and a shock is super-Alfvénic relative to the upstream solar wind, the shock will readily overtake the waves ($V_{\text{shock}} > V_{\text{ph}} \cos \theta_{kn}$). Thus upstream waves with these relatively low frequencies must be locally generated.

The source of these waves must be instabilities associated with energetic particles reflected by, or escaping from, the shock. Landau resonance with either electrons or ions flowing away from the shock can be ruled out because such an interaction requires a substantial component of the wave electric field parallel to **B**. This requirement means that the wave must propagate across, rather than along, the magnetic field, a requirement which is contrary to observations presented in this paper. Cyclotron resonance with energetic electrons also seems unlikely. Electron kinetic energies of ≥ 10 keV are required for first order cyclotron resonance. Typically, electrons at such high energies have not been detected by ISEE 3 [*Potter*, 1981; B. T. Tsurutani et al., manuscript in preparation, 1983].

The most likely mechanism is cyclotron resonance with reflected or escaping ions upstream of the shock, similar to the mechanism that has been successful in accounting for waves in the earth's foreshock. Extensive literature exists on the reflected [*Asbridge et al.*, 1968; *Gosling et al.*, 1978] and diffuse [*Lin et al.*, 1974; *West and Buck*, 1976; *Gosling et al.*, 1978; *Gurgiolo et al.*, 1981; *Bonifazi and Moreno*, 1981] ion populations and the instabilities responsible for the generation of these low-frequency right-hand waves [*Barnes*, 1970; *Sentman et al.*, 1981; *Gary et al.*, 1981].

The basic physical process involves a resonance between protons that outrun the shock, and waves in the upstream solar wind which are Doppler-shifted to appear at the gyrofrequency of the protons. There is a correspondence between the component of the proton kinetic energy parallel to the interplanetary magnetic field $W_{\|}$ and wave period T or frequency f. Because the particle and wave speeds are comparable to the solar wind speed, Doppler shifting of $W_{\|}$ and T into the spacecraft frame to produce the observed parallel energy $W_{\|_{sc}}$ and wave period T_{sc} must be taken into account.

Given basic interplanetary parameters, such as **B** and $\mathbf{V}_{sw}$ and also the wave V_{ph}, the relation between $W_{\|_{sc}}$ and T_{sc} can be derived. The proton velocity parallel to the field is $V_{\|_{sc}} = (2W_{\|_{sc}}/m)^{1/2}$. In the solar wind frame, the parallel proton velocity is $V_{\|} = V_{\|_{sc}} - V_{sw} \cos \theta_{BV}$. The ratio of this velocity to the parallel phase velocity of right-hand polarized waves $V_{ph_{\|}}$ determines the Doppler shift. At resonance, the wave frequency observed by the particle is equal to its gyrofrequency f_{gi}, so that $f_{gi}/f = V_{\|}/V_{ph} - 1$. This equation implies that particles are overtaking the waves so that anomalous Doppler-shifting leads to an apparent reversal in the sense of polarization. As a consequence, the waves are left-handed in the particle frame and have the same sense of rotation as the protons.

Using the relationship between the wave frequency in the spacecraft frame and in the solar wind frame given in equation (3), calculations, based on this approach, are presented in Figure 10. In this figure, the wave period in the solar wind and spacecraft frames are plotted as functions of the parallel proton energy (in the spacecraft frame). The curves assume $V_{sw} = 400$ km s^{-1}, $\theta_{BV} = 45°$, $B = 10$ nT and an approximate value of $V_{ph} = 100$ km s^{-1}. The latter value assumes $V_{ph} \simeq V_A$ for these low frequencies and corresponds to a solar wind density of 5 cm^{-3}.

The range of particle energies is chosen as being typical of those observed upstream of the terrestrial bow shock, i.e., 1–10 keV. Larger energies are included to account for long-period waves. A cutoff occurs at energies below 1 kev such that f_{gi}/f approaches zero. This cutoff arises when the particle velocity equals the wave velocity.

Waves propagating in the right-hand polarized mode are unaffected by the ion gyroresonance and continue to propagate at periods shorter than the ion gyroperiod, $T_{gi} = 6.6$ s for a field of 10 nT. At higher frequencies, the phase velocity begins to increase and the mode is recognizable as the dispersive whistler mode in which waves can propagate up to the electron gyrofrequency (280 Hz). Figure 10 shows that it is possible for waves to be generated by upstream ions at, and somewhat above, 1 Hz before being limited by the cutoff mentioned above.

A more accurate estimate of the cutoff frequency can be derived by departing from the assumption that $V_{ph_{\|}}$ is constant. For waves with frequencies above the ion gyrofrequency but well below the electron gyrofrequency, equation (2) can be used. The resonance condition can then be written as

$$V_{\|}/V_A = (1 + f_{gi}/f)(1 + f/f_{gi})^{1/2} \tag{5}$$

Solving $d(V_{\|}/V_A)/df = 0$ leads to a quadratic equation whose only positive root is

$$f_c = (f_{gi}/2)[1 + (1 + 8/f_{gi})^{1/2}]$$

For the values used to derive Figure 10, $f_{gi} \simeq 1$ and $f_c \simeq 2f_{gi}$. Thus the cutoff should be expected at $2f_{gi} = 0.30$ Hz in the solar wind frame. In the spacecraft frame, the cutoff would occur at

$$f_{\|_{sc}} = (1 + V_{sw} \cos \theta_{BV}/V_{ph_{\|}})f_c \tag{7}$$

which is approximately $(1 + 400 \cos 45°/100\ (1.73))\ (0.30) = 0.79$ Hz, i.e., in the vicinity of 1 Hz.

SUMMARY

Two types of waves have been detected upstream of interplanetary shocks. A higher frequency ($2 \times 10^{-1} - 2$ Hz, in spacecraft frame) whistler mode wave and a lower frequency ($\sim 5 \times 10^{-2}$ Hz) fast mode MHD wave. Both are typically circular or elliptically polarized right-hand waves which propagate along B within a cone of 15°. Because the solid angle subtended by this cone is less than 4% of the hemisphere, the waves are essentially propagating along **B**. It has been shown that the former wave is not a standing wave and that it is unlikely (especially at the highest frequencies, ~ 2 Hz) that the emissions are locally generated upstream of the shock. The only remaining possibility is that waves are generated at the shock and then propagate into the upstream region. These high-frequency waves have sufficient group velocities ($V_g \simeq 2V_{ph}$) to

outrun the shock (see equation (2)). The observation that the wave amplitudes are typically largest closest to the shock and decrease to the solar wind background within tens of seconds upstream of the shocks (presumably due to a combination of scattering and damping) are in support of this conclusion. One likely generation mechanism of these waves is cyclotron resonance with 100 eV to 1 keV shock electrons.

The lower frequency ($\sim 5 \times 10^{-2}$ Hz) waves detected up to 8 R_E upstream of the shock must be locally generated because the wave (group) speed is, in general, not large enough to allow for upstream propagation. These emissions must be generated by particles upstream of the shock. It has been demonstrated that the most probable source is 1–10 keV ions flowing away from the shock, in close analogy with the mechanism operating in front of the earth's bow shock.

Intense downstream waves were detected in most of the more than 100 shocks examined. In this paper, some of the events illustrated did not have obvious large amplitude waves in the downstream region (Figures 1, 2, and 5), but this feature is atypical. Since the primary concern of this paper is the upstream waves, our examples were chosen to illustrate (and study) these phenomena. There is some limited information in this paper about downstream waves. Examples can be found in Figures 6 and 7 and some discussion about the wave properties are in the text. However, a thorough detailed analysis will have to be postponed until a subsequent work.

Long duration wave events, such as that on days 315–316, 1978 (illustrated in Figures 7, 8, and 9) are not currently understood. It appears highly unlikely that a beam of ions, generated at or near the shock, could maintain sufficient anisotropy to cause wave generation some 0.04 AU from the source (E. Zweibel, personal communication, 1982). Reduction of the anisotropy should occur much more rapidly as the particles stream away from the shock and are scattered by the locally generated waves. It is clear that for these extraordinary cases, different sources for particle energy (and anisotropy) may be playing an important role in the distant upstream region.

Distinct changes in the spectra of upstream waves as a function of distance from the shock were noted. At regions close to the shock (Figure 9*c*), there is relatively greater power at high frequencies (10^{-1} to 10^{0} Hz), whereas further from the shock (Figures 9*a*, 9*b*) the wave power lies predominantly at the lower frequency end of the display (10^{-2} to 10^{-1} Hz). These spectral changes have distinct implications for the particles which are in resonance with the waves. It can be determined from Figure 10 that for the above wave frequency values, the lower energy ions (1–5 keV) play an important role close to the shock, whereas the more energetic particles ($E = 5$ keV to >100 keV) are important further from the shock. Stated a slightly different way, the above result implies that the upstream scale for energetic protons should be dependent on kinetic energy, a feature which is well established in the earth's foreshock [*Ipavich et al.*, 1981] and also for recent measurements upstream of interplanetary shocks [*Scholer et al.*, 1983]. Thus it is clear that studies involve both the wave and the energetic particle data for this event, and others like it, should provide some interesting results on first-order Fermi acceleration in interplanetary space.

Acknowledgments. We wish to thank J. T. Gosling and R. D. Zwickl of Los Alamos National Laboratory for kindly supplying the plasma data for parts of the analyses. We appreciate the helpful comments of D. H. Fairfield, K. P. Wenzel, C. F. Kennel, and the two referees. D. McDonald and L. Boren helped in the display and analysis of the wave data. We wish to express our appreciation for the excellent typing provided us by C. Gutierrez and C. Bowie. The work at Brigham Young University was supported in part by NASA under contract NAS 955-394. The work at the Jet Propulsion Laboratory represents one phase of research carried out under NAS 7-100 sponsored by the National Aeronautics and Space Administration.

The editor thanks M. Lee and D. H. Fairfield for their assistance in evaluating this paper.

REFERENCES

Abraham-Schrauner, B., Determination of magnetohydrodynamic shock normals, *J. Geophys. Res.*, *77*, 736, 1972.

Asbridge, J. R., S. J. Bame, and I. B. Strong, Outward flow of protons from the earth's bow shock, *J. Geophys. Res.*, *73*, 5777, 1968.

Barnes, A., Theory of generation of bow-shock-associated hydromagnetic waves in the upstream interplanetary medium, *Cosmic Electrodyn.*, *1*, 90, 1970.

Biskamp, D., Collisionless shock waves in plasmas, *Nucl. Fusion*, *13*, 719, 1973.

Bonifazi, C., and G. Moreno, Reflected and diffuse ions backstreaming from the earth's bow shock, 1, Basic properties, *J. Geophys. Res.*, *86*, 4397, 1981.

Burton, R. K., and R. E. Holzer, The origin and propagation of chorus in the outer magnetosphere, *J. Geophys. Res.*, *79*, 1014, 1974.

Eichler, D., Energetic particle spectra in finite shocks: The earth's bow shock, *Astrophys. J.*, *244*, 711, 1981.

Ellison, D. C., Monte Carlo simulation of charged particles upstream of the earth's bow shock, *Geophys. Res. Lett.*, *8*, 991, 1981.

Fairfield, D. H., Bow shock associated waves observed in the far upstream interplanetary medium, *J. Geophys. Res.*, *74*, 3541, 1969.

Fairfield, D. H., Whistler waves observed upstream from collisionless shocks, *J. Geophys. Res.*, *79*, 1368, 1974.

Fairfield, D. H., and W. C. Feldman, Standing waves at low Mach number laminar bow shocks, *J. Geophys. Res.*, *80*, 515, 1975.

Fisk, L. A., and M. A. Lee, Shock acceleration of energetic particles in corotating interaction regions in the solar wind, *Astrophys. J.*, *237*, 620, 1980.

Forman, M. A., First order Fermi acceleration of the diffuse ion population near the earth's bow shock, *Proc. 17th Int. Cosmic Ray Conf.*, *3*, 1467, 1981.

Gary, S. P., J. T. Gosling, and D. W. Forslund, The electromagnetic ion beam instability upstream of the earth's bow shock, *J. Geophys. Res.*, *86*, 6691, 1981.

Gosling, J. T., J. R. Asbridge, S. J. Bame, G. Paschmann, and N. Sckopke, Observations of two distinct populations of bow shock ions in the upstream solar wind, *Geophys. Res. Lett.*, *5*, 957, 1978.

Gurgiolo, C., G. K. Parks, B. H. Mauk, C. S. Lin, K. A. Anderson, R. P. Lin, and H. Reme, Non-**E** x **B** ordered ion beams upstream of the earth's bow shock, *J. Geophys. Res.*, *86*, 4415, 1981.

Heppner, J. P., M. Sugiura, T. L. Skillman, B. G. Ledley, and M. Campbell, OGO-A magnetic field observations, *J. Geophys. Res.*, *72*, 5417, 1967.

Holzer, R. E., T. G. Northrop, J. V. Olsen, and C. T. Russell, Study of waves in the earth's bow shock, *J. Geophys. Res.*, *77*, 2264, 1972.

Hoppe, M. M., and C. T. Russell, Particle acceleration at planetary bow shock waves, *Nature*, *295*, 41, 1982.

Hoppe, M. M., C. T. Russell, L. A. Frank, T. E. Eastman, and E. W. Greenstadt, Upstream hydromagnetic waves and their association with backstreaming ion populations: ISEE 1 and 2 observations, *J. Geophys. Res.*, *86*, 4471, 1981.

Hoppe, M. M., C. T. Russell, T. E. Eastman, and L. A. Frank, Characteristics of the ULF waves associated with upstream ion beams, *J. Geophys. Res.*, *87*, 643, 1982.

Ipavich, F. M., A. B. Galvin, G. Gloeckler, M. Scholer, and D. Hovestadt, A statistical survey of ions observed upstream of the earth's bow shock: Energy spectra, composition, and spatial variation, *J. Geophys. Res.*, *86*, 4337, 1981.

Jokipii, J. R., A model of Fermi acceleration of shock fronts with an application to the earth's bow shock, *Astrophys. J.*, *143*, 961, 1966.

Karpman, V. I., Structure of the shock front propagating at an angle to a magnetic field in a low-density plasma, *Sov. Phys. JETP Engl. Transl.* *8*, 715, 1964.

Kennel, C. F., F. L. Scarf, F. V. Coroniti, E. J. Smith, and D. A. Gurnett, Nonlocal plasma turbulence associated with interplanetary shocks, *J. Geophys. Res.*, *87*, 17, 1982.

Lee, M. A., Coupled hydromagnetic wave excitation and ion acceleration upstream of the earth's bow shock, *J. Geophys. Res.*, *87*, 5063, 1982.

Lin, R. P., C. I. Meng, and K. A. Anderson, 30- to 100-keV protons upstream from the earth's bow shock, *J. Geophys. Res.*, *79*, 489, 1974.

Olsen, J. V., R. E. Holzer, and E. J. Smith, High-frequency magnetic fluctuations associated with the earth's bow shock, *J. Geophys. Res.*, *74*, 4601, 1969.

Perez, J. K., and T. G. Northrop, Stationary waves produced by the earth's bow shock, *J. Geophys. Res.*, *75*, 6011, 1970.

Potter, D. W., Acceleration of electrons by interplanetary shocks, *J. Geophys. Res.*, *86*, 11,111, 1981.

Russell, C. T., D. D. Childers, and P. J. Coleman, Jr., OGO 5 observations of upstream waves in the interplanetary medium: Discrete wave packets, *J. Geophys. Res.*, *76*, 845, 1971.

Russell, C. T., E. J. Smith, B. T. Tsurutani, J. T. Gosling, and S. J. Bame, Multiple spacecraft observations of interplanetary shocks: Characteristics of the upstream ULF turbulence, *Sol. Wind Proc. Conf., 5th*, in press 1983.

Sanderson, T. R., R. Reinhard, and K.-P. Wenzel, Observations of upstream ions and low-frequency waves on ISEE 3, *J. Geophys. Res.*, *88*, 85, 1983.

Scholer, M., F. M. Ipavich, G. Gloeckler, and D. Hovestadt, Acceleration of low-energy protons and alpha particles at interplanetary shock waves, *J. Geophys. Res.*, *88*, 1977, 1983.

Sentman, D. D., J. P. Edmiston, and L. A. Frank, Instabilities of low-frequency parallel propagating electromagnetic waves in the earth's foreshock region, *J. Geophys. Res.*, *86*, 7487, 1981.

Smith, E. J., and B. T. Tsurutani, Magnetosheath lion roars, *J. Geophys. Res.*, *81*, 2261, 1976.

Sonnerup, B. U., and L. J. Cahill, Jr., Magnetopause structure and attitude from Explorer 12 observations, *J. Geophys. Res.*, *72*, 171, 1967.

Stix, T. H., *The Theory of Plasma Waves*, McGraw-Hill, New York, 1962.

Terasawa, T., Origin of 30–100 keV protons observed in the upstream region of the earth's bow shock, *Planet. Space Sci.*, *27*, 365, 1979.

Terasawa, T., Energy spectrum of ions accelerated through Fermi process at the terrestrial bow shock, *J. Geophys. Res.*, *86*, 7595, 1981.

Thorne, R. M., E. J. Smith, R. K. Burton, and R. E. Holzer, Plasmaspheric hiss, *J. Geophys. Res.*, *78*, 1581, 1973.

Tidman, D. A., and N. A. Krall, *Shock Waves in Collisionless Plasmas*, John Wiley, New York, 1971.

Tsurutani, B. T., and P. Rodriguez, Upstream waves and particles: An overview of ISEE results, *J. Geophys. Res.*, *86*, 4317, 1981.

Tsurutani, B. T., E. J. Smith, K. R. Pyle, and J. A. Simpson, Energetic protons accelerated at corotating shocks: Pioneer 10 and 11 observations from 1 to 6 AU, *J. Geophys. Res.*, *87*, 7389, 1982.

West, H. I., Jr., and R. M. Buck, Observations of >100-keV protons in the earth's magnetosheath, *J. Geophys. Res.*, *81*, 569, 1976.

(Received November 29, 1982;
revised February 28, 1983;
accepted March 24, 1983.)